

# Digital Wavefront Measuring Interferometer for Testing Optical Surfaces and Lenses

J. H. Bruning, D. R. Herriott, J. E. Gallagher, D. P. Rosenfeld, A. D. White, and D. J. Brangaccio

A self-scanned 1024 element photodiode array and minicomputer are used to measure the phase (wavefront) in the interference pattern of an interferometer to  $\lambda/100$ . The photodiode array samples intensities over a  $32 \times 32$  matrix in the interference pattern as the length of the reference arm is varied piezoelectrically. Using these data the minicomputer synchronously detects the phase at each of the 1024 points by a Fourier series method and displays the wavefront in contour and perspective plot on a storage oscilloscope in less than 1 min (Bruning *et al.* Paper WE16, OSA Annual Meeting, Oct. 1972). The array of intensities is sampled and averaged many times in a random fashion so that the effects of air turbulence, vibrations, and thermal drifts are minimized. Very significant is the fact that wavefront errors in the interferometer are easily determined and may be automatically subtracted from current or subsequent wavefronts. Various programs supporting the measurement system include software for determining the aperture boundary, sum and difference of wavefronts, removal or insertion of tilt and focus errors, and routines for spatial manipulation of wavefronts. FFT programs transform wavefront data into point spread function and modulus and phase of the optical transfer function of lenses. Display programs plot these functions in contour and perspective. The system has been designed to optimize the collection of data to give higher than usual accuracy in measuring the individual elements and final performance of assembled diffraction limited optical systems, and furthermore, the short loop time of a few minutes makes the system an attractive alternative to constraints imposed by test glasses in the optical shop.

## I. Introduction

Optical interferometry has long been used to examine the surfaces of lens elements and the quality of the finished lens. The advent of the laser has made interferometers more convenient to use, but the sensitivity has not been increased. The  $\lambda/2$  contour interval in the fringe pattern of a lens surface in a Twyman-Green interferometer is not sufficient for many applications. Lenses for photolithography in integrated circuits are a case in point. Here the lenses may have twenty or more surfaces. The converging spherical wavefront in image space produced by a point source in object space must have errors less than  $\lambda/4$ . This requires better than a  $\lambda/10$  figure on each of the surfaces in the lens and, of course, requires an even higher measurement accuracy in order to fabricate the surfaces. This type of accuracy is not provided by conventional interferometry or test glasses.

Systems have been described in which interferograms are photographed, the photographs scanned optically, and densitometer readings processed by computer to obtain more sensitive wavefront measurements. These systems may be inaccurate or inconvenient for the following reasons.

- (1) Nonlinearity of the photographic process introduces distortion at points not centered on fringe extrema.
- (2) A tilt of the reference to obtain close spaced whole fringes causes distortion or other lateral measurement error to be converted to phase errors.
- (3) It is difficult to average wavefronts to eliminate the effects of atmospheric turbulence and drift.
- (4) It is difficult to determine and compensate for interferometer defects.
- (5) The process takes so much time and effort that it is generally not used as a routine process control system.

This paper describes a system for measuring components and lenses to a small fraction of a fringe by averaging many wavefronts to eliminate the effects of turbulence and noise. The errors of the interferometer are explicitly measured and compensated before the wavefront, point spread function, modulation transfer function, or optical transfer function are displayed in contour map and perspective plot.

J. E. Gallagher is with McDonnell Douglas Corporation, Huntington Beach, California 92646; the other authors are with Bell Laboratories, Murray Hill, New Jersey 07974.

Received 24 May 1974.

Only 1 min or 2 min are required to sample automatically the fringe field, calculate the phases, and plot the desired output, making the system convenient for routine process control.

## II. General Interferometer System

The general interferometer system consists of a modified Twyman-Green interferometer using a single-frequency laser source. An optical system is used in the sample arm of the interferometer to match the incident wavefront either to the surface of an element under test or to a finished lens at the proper conjugates. The fringe pattern is imaged onto a detector having a  $32 \times 32$  array of diodes that sample the image. The diode array signals are displayed on a television screen so that the fringes can be adjusted, the image centered and magnified to fill properly the field. The diode array signals are also digitized and sent to a minicomputer where many repeated samples can be processed to measure the phase at each point in the wavefront. A piezoelectrically driven mirror is used in the reference arm of the interferometer so that repeated samples can be taken at different phases in a detection system that tends to minimize errors caused by noise, drift, atmospheric turbulence, and nonlinearities. An A to D converter changes the diode signals into digital information for the computer, and a D to A converter changes computer signals to analog voltages to drive the piezoelectric element to the desired position.

The wavefront is detected by measuring the intensity over the array of 1024 points repeatedly after introducing incremented phase shifts in the reference arm. The intensity at each of the sampling diodes varies sinusoidally as the phase shift introduced is varied linearly. The phase shift at each diode relative to the central diode, for example, is a measure of the relative phase at that point in the wavefront. A Fourier series method is used to calculate this phase array which is then processed to present the desired display.

### A. Phase Detection Technique

Consider a Twyman-Green interferometer as shown in Fig. 1. Assuming perfect components, the relative reference and test wavefronts are given, respectively, by

$$w_1 = a \exp(2ikl), \quad k = 2\pi/\lambda,$$

$$w_2 = b \exp[2ikw(x, y)],$$

where  $l$  is the mean pathlength from the beam splitter to the reference surface, and  $w(x, y)$  represents the two-dimensional profile of the test surface which is sought. The amplitudes of the interfering wavefronts are  $a$  and  $b$ , respectively. From this we find that the intensity distribution in the interference pattern or fringe pattern is

$$I(x, y, l) = (w_1 + w_2)(w_1 + w_2)^* = a^2 + b^2 + 2ab \cos 2k[w(x, y) - l]. \quad (1)$$

The spacing between intensity minima or fringes

corresponds to an optical path difference (OPD) in the two arms of the interferometer of  $\lambda/2$  as verified by Eq. (1). What we are really interested in is the function  $w(x, y)$ , be it a surface or OPD. It is also clear from Eq. (1) that  $I(x, y)$  is a sinusoidal function of  $l$  for all  $(x, y)$  within the fringe pattern.

Consider then, an alternative representation for Eq. (1),

$$I(x, y, l) \triangleq a_0 + a_1 \cos 2kl + b_1 \sin 2kl. \quad (2)$$

This is a Fourier series with the dc term and first harmonics only. It is understood that the coefficients are functions of  $x$  and  $y$ . In the sampled data sense, the coefficients at each  $(x, y)$  are found by sequentially sampling the fringe pattern and making use of the orthogonality properties of the trigonometric functions:

$$a_0 = \frac{1}{np} \sum_{i=1}^{np} I(x, y, l_i) = a^2 + b^2, \quad (3)$$

$$a_1 = \frac{2}{np} \sum_{i=1}^{np} I(x, y, l_i) \cos 2kl_i = 2ab \cos 2kw(x, y), \quad (4)$$

$$b_1 = \frac{2}{np} \sum_{i=1}^{np} I(x, y, l_i) \sin 2kl_i = 2ab \sin 2kw(x, y); \quad (5)$$

thus,

$$2kw(x, y) = \tan^{-1}(b_1/a_1) \text{ mod } 2\pi. \quad (6)$$

$$l = l_i = \frac{i\lambda}{n2} \quad i = 1, 2, \dots, np.$$

The integer  $p$  denotes the number of periods (fringes) over which the interference pattern is sampled and  $n$  the quantization of each period. Hence, for each point in the interference pattern, the phase or wavefront can be found within some multiple of  $2\pi$ . Knowing that  $w(x, y)$  is a continuous function of  $(x, y)$  within the aperture,  $\lambda/2$  discontinuities in  $w(x, y)$  are easily resolved.

It is interesting to note that in this case, the Fourier series representation is precisely an autocorrelation or synchronous detection technique. The coefficients so determined represent the best approximation in a least squares sense to  $I(x, y, l)$ . Since this is a synchronous detection technique, we are sensitive

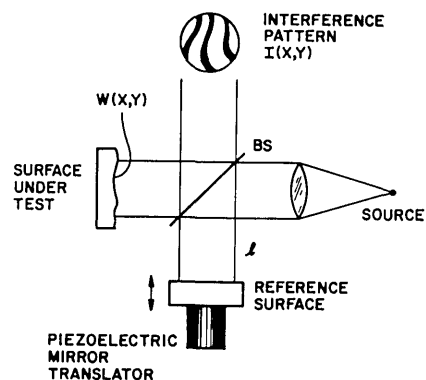


Fig. 1. Twyman-Green interferometer with piezoelectric path-length control in reference arm.

to drifts and turbulence with frequency components near the carrier frequency  $2kl(t)$ , the reciprocal of the sampling time. The sampling time in this case is the time required for the reference mirror to move  $p\lambda/2$  or  $p$  periods of the function  $I[x,y,l(t)]$ . Sensitivity to this source of error is minimized by sampling  $I(x,y,l)$  in a pseudorandom order. Randomizing the order of data sampling transforms a drift with a strong component near the carrier into one with frequency components uniformly distributed over a very wide frequency spectrum. If data are accumulated over many periods ( $p$  large) in the presence of slow but sizable drifts, the detection technique will not yield results that improve with sampling time. However, if many wavefronts are averaged, each taken from data accumulated over relatively short time intervals with respect to drifts ( $p$  small), results improve with more data. This results because slow drifts tend to be linear, and these effects may be removed from the individual wavefronts by calculating and extracting residual tilts and focus errors.

The drift situation may be assessed during each run which normally consists of 4 periods of 25 samples per period ( $p = 4, n = 25$ ). After data from each period are accumulated, a vector is drawn on the storage oscilloscope from the last pair of partial sums to the current pair. The  $x$  and  $y$  coordinate pairs of the vectors correspond to unnormalized forms of  $a$ , and  $b$ , respectively [c.f. Eqs. (4) and (5)]. At the end of each run, if the vectors do not follow a straight line, this indicates there is drift and the measurement is repeated.

## B. Error Sources

There are a number of sources of error that must be considered in the system. Noise in the laser source, electrical noise in the detectors, nonlinear fringe contours caused by extraneous beams, mechanical drifts, and atmospheric turbulence can all affect the system performance.

When attempting to measure a wavefront to  $\lambda/100$ , some of these factors, occasionally ignored, can play a significant role. The laser source is one component that must be carefully considered. First, the output power must possess good short-term stability. This also implies that the fringe pattern contrast, and hence the coherence properties of the laser, must also maintain short-term stability. The latter situation either requires a single frequency stabilized laser or the ability to keep the path difference in the two arms of the interferometer constant and equal to some integer multiple of the cavity length of the laser. Although more expensive, the stabilized laser operating in a single longitudinal mode is preferred since all pathlength restrictions are removed, and all optics preceding the test surface may remain fixed.

With good source stability, the wavefront system yields extremely reproducible results. Two successive runs produce an rms difference of less than  $10^{-4}\lambda$ . This means that it always reports exactly the fringe pattern it sees. However, under various circumstances, the fringe pattern seen may not accu-

rately represent the desired interfering wavefronts. Such is the case when the interference pattern is composed of more than two interfering wavefronts. While this type of interference can be greatly reduced with polarization filtering, we should consider the effect of interfering three wavefronts. Consider then the following three wavefronts:

$$w_1 = \exp(i\rho) - \text{from reference arm;}$$

$$w_2 = \exp(i\tau) - \text{from test arm;}$$

$$w_3 = \epsilon \exp(i\eta) - \text{extraneous.}$$

No loss of generality is incurred by setting the reference wavefront phase identically zero. With this, the fringe pattern takes the form

$$I(x,y) = \alpha + \beta \cos(\tau - \phi),$$

where  $\alpha = \text{constant}$ ,

$$\beta = \text{fringe contrast} \leq 1.$$

The function  $\phi(x,y)$  may introduce a distortion in the fringe pattern  $I(x,y)$  and in the wavefront  $\tau(x,y)$  which we are trying to measure. The magnitude of this distortion is easily shown to be related to the extraneous wavefront  $\epsilon \exp i\eta$  by

$$\phi = \tan^{-1}[(\epsilon \sin\eta)/(1 + \epsilon \cos\eta)].$$

The distortion, however, disappears if  $\eta$  is either a rapidly varying function of position or a constant. An example will illustrate the point that under special circumstances there could be a substantial error. Consider an uncoated surface in the test arm and an extraneous reflection from a surface coated with a single layer AR coating. Thus, the reflectivity of the test surface is 0.04 and the reflectivity of the extraneous surface 0.01. This leads to an amplitude ratio  $\epsilon = 0.5$ . Assume also that the extraneous wavefront is a slowly varying function of position and takes on relative values including  $\pm\pi/2$ . Thus over the aperture there could be as much as  $\phi = \pm\tan^{-1}(0.5)$  for a total of  $\lambda/7$  error in the wavefront. This effect (although very much smaller than  $\lambda/7$ ) has been observed when testing bare glass surfaces, but disappears when the test surfaces are reflective coated.

This source of error is not due to the detection technique but, rather, a result of the extended coherence properties of the laser source. The presence of extraneous wavefronts is easily checked by running the system with the test surface removed. If the am-

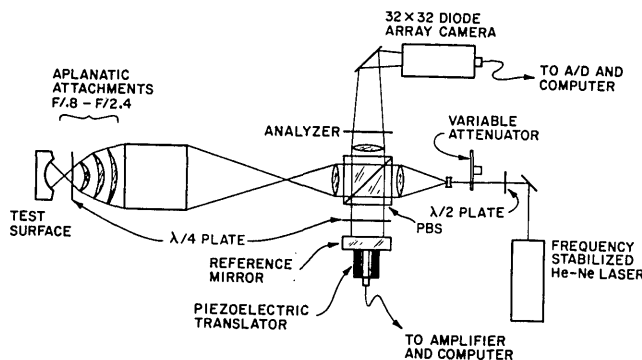


Fig. 2. Twyman-Green digital wavefront measuring interferometer.

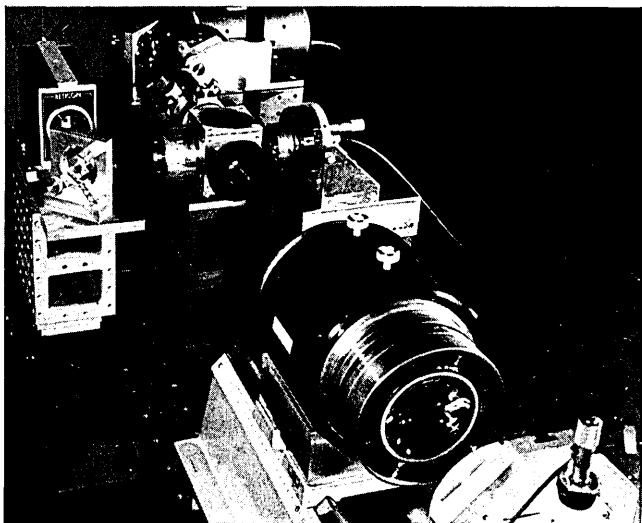


Fig. 3. Detailed view of interferometer.

plitude of an extraneous wavefront is at all significant, a well formed fringe pattern will be plotted on the storage oscilloscope. If not, the pattern plotted will appear as noise.

Data averaging is very effective in eliminating detector noise and atmospheric turbulence of a rapid nature. Slow drifts in the mechanical system and slowly changing atmospheric refraction are not completely cancelled by very long averaging. This is because the slow changes may be synchronous with repetitions in the phase cycles of the reference beam. Improved cancellation of this type of noise is achieved by making a number of short averaged runs, recovering the wavefronts from each run and averaging these wavefronts. This type of averaging can be automatically continued for long periods with corresponding reductions in noise.

### III. Interferometer

#### A. General

The interferometer as currently configured is shown schematically in Fig. 2 and pictorially in Fig. 3. Experience with earlier systems has demonstrated that accuracies in the  $\lambda/100$  range necessitate a stable single frequency source. Use of a lamb-dip stabilized single frequency laser satisfies the frequency stability requirement and also allows operation of the interferometer at widely differing pathlengths between the two arms—not simply multiples of the laser cavity length. This allows the length of the reference arm to remain fixed at approximately 5 cm.

Figuring of surfaces and final testing of elements involve testing unsilvered or antireflection coated surfaces. The latter case requires an economic use of available light since reflectivities may be below 1%. Under these conditions, the use of a polarizing beam splitter (PBS) represents the optimum solution in terms of minimum light loss.

The polarized laser source is followed by a  $\lambda/2$

plate. Rotation of this orients the incident linear polarization at an angle  $\phi_i$  from the vertical direction. This controls the division of light intensity between the test and reference arms, which are, respectively,

$$I_{\text{TEST}} = I_0 \sin^2 \phi_i,$$

$$I_{\text{REF}} = I_0 \cos^2 \phi_i.$$

These two signals pass through  $\lambda/4$  plates twice, which rotates their respective polarization  $90^\circ$  allowing unattenuated passage into the viewing arm. An important aspect of the PBS- $\lambda/4$  plate configuration is that reflected light from all surfaces preceding the final surface of each waveplate is rejected from the viewing arm by the PBS. This may be significant when complex optical systems are used or tested in the sample arm. In this case, the  $\lambda/4$  plate is placed immediately in front of the surface under test or the reference mirror. The  $\lambda/4$  plate in the sample arm may be used in converging light up to about  $F/2$  without appreciable nonuniformity in amplitude of the returned beam.<sup>2</sup> Interference cannot take place unless there are components from both arms of the same polarization. The analyzer preceding the detector generates components of both polarizations from the two orthogonally polarized return beams. The orientation of the analyzer  $\phi_A$  with respect to the vertical direction controls the relative intensities of the return beams in a common polarization direction and thus the fringe pattern contrast. This is maximized when the component intensity of the two returned beams are equal. If we assume the mirror in the reference arm has unit reflectivity and the test surface has a reflectivity of  $R$ , the above condition requires

$$RI_{\text{TEST}} \cos^2 \phi_A = I_{\text{REF}} \sin^2 \phi_A, \quad (7)$$

or

$$RI_0 \sin^2 \phi_i \cos^2 \phi_A = I_0 \cos^2 \phi_i \sin^2 \phi_A,$$

hence,

$$\phi_A = \tan^{-1}(R \tan \phi_i). \quad (8)$$

The maximum signal is then obtained when the incident polarization  $\phi_i$  is appropriately chosen. Maximizing the reference signal subject to the constraint (8) yields the following:

$$\frac{\partial}{\partial \phi_i} (\cos^2 \phi_i \sin^2 \phi_A) = \frac{\partial}{\partial \phi_i} \left[ \frac{R \sin^2 \phi_i}{(1 + R^2 \tan^2 \phi_i)^{1/2}} \right] = 0,$$

or

$$\phi_i = \tan^{-1}(1/R)^{1/2}, \quad (9)$$

$$\phi_A = \tan^{-1}(R)^{1/2}. \quad (10)$$

Inserting Eq. (9) and Eq. (10) into Eqs. (7) we find that the maximum signal at the detector is

$$I_{\text{max}} = I_0 [R/(1 + R)]. \quad (11)$$

This final result is quite significant when  $R$  is small. If we compare  $I_{\text{max}}$  above (obtained with a PBS) with  $I_{\text{max}}$  obtained with a nonabsorbing 50/50 nonpolarizing beam splitter, we find a factor of 4 more light with small  $R$  and a factor of 2 when  $R \rightarrow 1$ . This result has permitted the use of a 300- $\mu$ W laser source even when  $R \sim 0.01$ . Under most conditions the light must be attenuated.

When another surface of different reflectivity  $R$  is



Fig. 4. PDP8/I computer system.

tested, the angles  $\phi_i$  and  $\phi_A$  are adjusted appropriately as above. The peak light level is then adjusted with a variable attenuator so that the detector is operated just below saturation. This yields the largest dynamic range without clipping. The diode array detector operates in a charge storage mode so that light flux is integrated linearly over the frame scan time. The computer controls the scanning by delivering clock pulses to the array. This rate is limited at present by the computer (PDP8/I) to 20  $\mu$ sec per element or approximately 20 msec per frame. A self-scanned diode array detector is preferred over a conventional sampled video system because this allows data input to be limited only by the computer. The computer does not have to be synchronized to a data rate set by the standard vidicon line rate. Since the array camera is clocked by the computer, synchronizing problems are absent. Because of charge storage, the array must be cleared or refreshed before a data frame is stored. During the refresh time, the reference mirror is moved to a new position by the piezoelectric transducer and given time to settle down mechanically. Its position is determined by the control program that sets a D/A converter and high voltage amplifier connected to the transducer. Simultaneous with this, the intensities from the last frame are accumulated in the Fourier series. For this application, charge storage operation is highly desirable since this yields a 1000-fold increase in sensitivity over discrete photodiodes and integrates out light variations above 100 Hz. Furthermore, since the

diode active area is half of the matrix area, we have spatial integration as well. For testing lenses and surfaces, the  $32 \times 32$  quantization of the wavefront is adequate since the polishing process does not tend to introduce rapid local departures from sphericity. The computer system is shown in Fig. 4, and the array camera interface is diagrammed in Fig. 5.

#### B. Interferometer Errors

The minicomputer makes it possible to store a number of wavefronts. This makes it practical to measure the errors of the interferometer and subtract them automatically from each subsequent measurement. This then relaxes somewhat the precision required of the individual components making up the interferometer. For example, if the wavefront of a test surface were taken and stored and then subtracted from the wavefront obtained from a perfect standard of the same radius, the interferometer errors could be arbitrarily large. If the standard surface were of a different radius than the test surface, one has to consider the effect of the change in shape of the wavefront as it propagates over a distance equal to the difference in radii of the test and reference surfaces. Consideration of this leads to an over-all error specification for the interferometer parts of  $\leq 1\lambda$  before errors approaching  $\lambda/100$  enter the resultant wavefront. This is quite a generous tolerance. Clearly  $\lambda/100$  errors on a test surface cannot be detected in the presence of  $1\lambda$  errors in the interferometer without wavefront subtraction.

#### IV. Software

Software for the wavefront measurement system has been written in modular form for use with a disk operating system. The executive program is the PS/8 system supplied by Digital Equipment Corporation. This enables easy manipulation of named data files, program generation, editing, debugging, and assembly. Principally, this facilitates serial execution of some predetermined list of programs

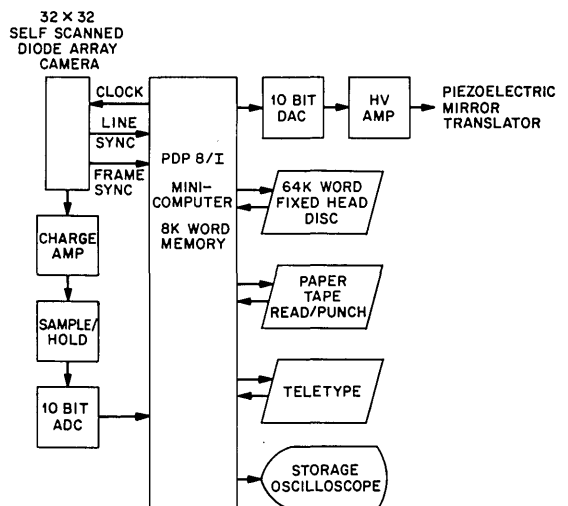


Fig. 5. Computer interface and peripherals.

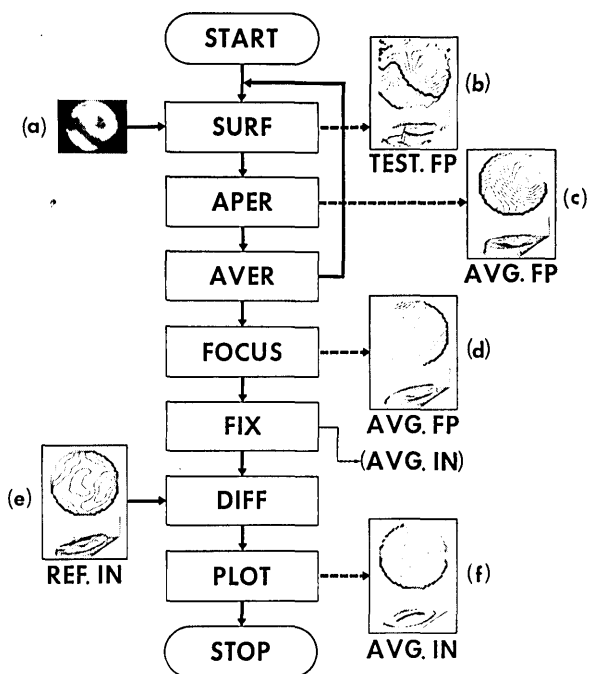


Fig. 6. Program flow for measurement of a lens surface: (a) appearance of digitized fringe pattern as seen on monitor oscilloscope; (b) output of raw phases after data accumulation showing  $\lambda/2$  discontinuities in the wavefront; (c) wavefront after aperture determination and discontinuity removal; (d) wavefront after focus and tilt errors are removed; (e) stored wavefront representing interferometer errors; (f) corrected wavefront display in  $\lambda/20$  contours on the surface under test.

(chaining) that are stored on the disk system. This is necessary since all the programs required cannot reside in core storage (8K 12-bit words) simultaneously. The program sequence for measuring a wavefront is illustrated in Fig. 6 with the state of the wavefront at each step displayed. At operator option, the program chain may be entered at any point. Each program and file name will be briefly described as it is encountered. The following sequence illustrates typically the testing of a surface.

#### A. Surf

R SURF is typed in at the teletype keyboard, and the operating system searches the disk file directory for program SURF and brings this program into core storage and starts execution. This is the main control program for data acquisition. This delivers clock pulses to the diode array for serial data entry into the A/D converter, controls the movable mirror, and performs the calculation of the phases using the Fourier series method described previously. Before the data are sampled, certain options are requested, such as the number of sets of data within a run to be taken and the number of runs to be averaged. Options affecting other programs are also entered at this point and will be described as they occur. Default options are used if none are specified. After the data have been accumulated in the Fourier series, the arc-

tangents are computed modulo  $2\pi$ . This represents the raw wavefront data output from SURF. These data are in floating point format and are written automatically onto the file named TEST.FP. The file extension .FP indicates that the file is in three-word floating point format, thus requiring  $3 \times 1024$  twelve-bit words of storage. The appearance of the wavefront at this point (although it is not usually displayed) is shown in Fig. 6(b).

#### B. APER

The  $\lambda/2$  discontinuities in the wavefront and the undefined aperture in the previous figure are quite apparent. The APER program resolves these ambiguities [cf., Fig. 6(c)]. Degree of modulation of the fringe pattern at each of the 1024 points is determined by computing the peak-to-peak magnitude of the signal

$$2ab/(a + b)^2 = (a_1^2 + b_1^2)^{1/2}/[a_0 + (a_1^2 + b_1^2)^{1/2}]$$

[cf., Eqs. (1)–(5)]. Clearly points within the aperture will have a larger modulation than points outside. This fact is used to define the aperture. Nominally a threshold value of 15–20% defines the aperture well. One must also make sure that the imaging optics proceeding the detector are arranged to allow the aperture to be imaged on the diode array, otherwise the aperture becomes poorly defined due to Fresnel diffraction. This also results in phase errors at the aperture boundary. The aperture determination is made by comparison of the relative modulation with the threshold value retained in the APER program which is chained in automatically following SURF. Points outside the aperture are assigned a small constant negative phase. Points inside the aperture are then examined for discontinuities of  $2\pi$  or  $\lambda/2$  by a simple algorithm. If the phase of two adjacent points differs by more than  $\pi$ ,  $\pm 2\pi$  is added to one until continuity is reestablished. All points are treated in this way until no more ambiguities exist. This tacitly assumes that the slope in the measured wavefront does not exceed  $\lambda/4$  between diodes. This range could be extended by considering a slightly more complex continuity algorithm, but for most cases of practical interest (high quality optics—for which the system was built), this is adequate. After continuity is established and the aperture boundary fixed, the wavefront data are rewritten onto the file TEST.FP

#### C. AVER

The data collection scheme permits higher accuracies to be achieved by processing more data. This may be done by averaging many wavefronts or accumulating more data for each wavefront in the Fourier coefficients, or both. The average of a group of wavefronts is stored under the file name AVG.FP. The first word of the file contains a number denoting the number of files in the current average so that as

the average is updated, the files are weighted appropriately. This represents a cumulative average, and hence with each successive run, the weighted average of TEST.FP and AVG.FP is returned to AVG.FP. Initially unless specified otherwise, as an option in SURF, AVG.FP is zeroed before AVER is executed.

#### D. FOCUS

A fringe pattern is often difficult to interpret because it contains the desired information in the presence of extraneous tilt and focus components in addition to errors in the interferometer. The former components are difficult to visually separate from the latter. When the wavefront data are in memory of the computer, tilt and focus are easily extracted. The wavefront at each point within the aperture ( $x_i, y_j$ ) may be written as

$$w(x_i, y_j) = w_0(x_i, y_j) + A + Bx_i + Cy_j + D(x_i^2 + y_j^2). \quad (12)$$

$w(x_i, y_j)$  is the phase at  $(i, j)$  as measured, and  $w_0(x_i, y_j)$  is the phase with the dc shift ( $A$ ), tilts ( $B$ ) and ( $C$ ), and focus ( $D$ ) removed. To find  $w_0$ , the coefficients  $A$  to  $D$  must be determined. These are found by minimizing  $w$  with respect to  $A, B, C$ , and  $D$  in the least squares sense at all points within the aperture. The coefficients are determined, and their value in wavelengths is printed out on the teletype. The new wavefront  $w_0(x_i, y_j)$  now replaces the previous contents of AVG.FP. This operation is a vital part of accurate wavefront measurements since it allows all wavefronts to be compared in the same manner. The test piece does not then have to be painstakingly inserted and adjusted in the interferometer since these fixturing errors are removed. The appearance of the wavefront after FOCUS is as shown in Fig. 6(d). The option /J when entered at the start of SURF will cause the program chain to bypass the FOCUS program.

The wavefront representation (12) could be modified to include other coefficients such as the primary aberration coefficients. This would be useful for evaluating design performance if  $w(x, y)$  represents the OPD of a lens under test. Aspheric coefficients could be added to Eq. (12) when  $w(x, y)$  represents the surface of a lens. Once these are found, they can be checked against the design values during figuring of an aspheric, thus obviating the need for a null corrector in the interferometer. Furthermore, if elements of a very high quality lens are measured prior to assembly, the small aspheric coefficients of the measured surfaces could be entered into the lens design program and new airspaces found that more closely match the real surface shapes and optimize the performance. This latter application is a fine tuning scheme that would be employed only in the most exacting of requirements.

#### E. FIX

All calculations involving summations and mathematical manipulations require floating point repre-

sentation to maintain the highest accuracy throughout. For subtraction and plotting of wavefronts, fixed point or integer format is used. Floating point files are fixed and rewritten onto the disk system in fixed point with the file extension .IN. This program will also float fixed point files and assign the extension .FP when called separately. This feature is useful if combinations of integer files require data manipulation. Data files to be retained are saved in this integer format for storage economy.

#### F. DIFF

When surfaces are tested they are compared to a reference surface. The reference wavefront is run and stored in REF.IN. The system is run again with the test surface (AVG.IN), and DIFF computes AVG.IN-REF.IN and places this in AVG.IN. This is the surface topography without the interferometer errors and is shown in Fig. 6(e). When a lens is being tested, REF.IN is the wavefront without the test lens, and AVG.IN is the wavefront with the test lens in the interferometer. The difference of these (REF.IN-AVG.IN) gives the OPD of the lens in single pass at that particular field position. This is also extensively used when the optician wants to see, for instance, the effect of changing his polishing stroke. The effect of changing the stroke is simply displayed as the difference of surface wavefronts before and after the stroke was changed. This program automatically takes the indicated difference if /D is entered as an option before SURF is run.

#### G. PLOT

When data files are in integer format they may be displayed on a storage oscilloscope. PLOT plots equiphase contours of wavefronts at  $\lambda/20$  contour intervals, which represents in fact, again, a fringe pattern. In appearance this resembles multiple beam patterns because of the narrowness of the fringes. The contour interval is alterable when PLOT is called separately.

#### H. 3-D

A fringe pattern or contour map without numerical markings gives no indication as to whether the extrema are maxima or minima. 3-D generates and displays an oblique projection of the same data below the contour plot so that these ambiguities are resolved. These two plots provide a clear indication of the location and magnitude of wavefront or OPD deformations.

Other programs used will be described in context.

### V. Calibration

It is generally felt that a surface can be made to the accuracy with which it can be measured. This also, of course, assumes that the measured results can be appropriately interpreted. This has been a major goal in the present program—the unambiguous display of measured results that can show the technician in the optical shop where material must be removed.

When a surface or lens is measured, its wavefront

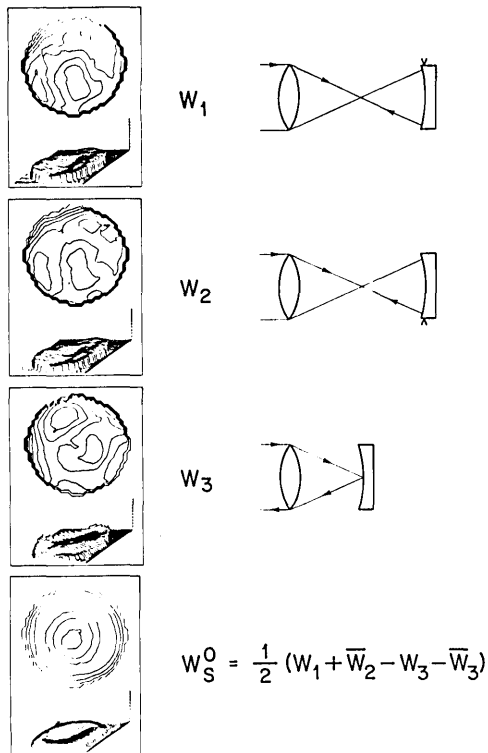


Fig. 7. Wavefronts processed for absolute calibration of interferometer.  $W_1$ ,  $W_2$ , and  $W_3$  are input wavefronts,  $W_5$  represents the test surface in the absence of interferometer errors (see text).

is compared to that obtained from a perfect reference surface—the difference indicating the state of the wavefront or surface under test. The absolute accuracy of the resultant is only as good as the reference surface, which in the present setup is better than  $\lambda/50$ . The repeatability far exceeds this.

An absolute calibration means has recently been described that is ideally suited to a real time digital interferometer.<sup>3</sup> It requires a facility for mathematically manipulating three wavefronts  $W_1$ ,  $W_2$ , and  $W_3$ . These are shown in Fig. 7.  $W_1$  is the wavefront obtained with the test surface oriented in some particular manner.  $W_2$  is the wavefront obtained as before but with the test surface rotated  $180^\circ$  about its axis. Finally  $W_3$  is obtained by placing the apex of the test surface at the focus of the collimator. If we introduce the following notation, the results will become clear.

$$W_1 = W_R^0 + W_T^0 + W_S^0,$$

$$W_2 = W_R^0 + W_T^0 + W_S^\pi,$$

$$W_3 = W_R^0 + \frac{1}{2}(W_T^0 + W_T^\pi),$$

where

$W_R^\alpha$  = wavefront contribution from the reference arm;

$W_T^\alpha$  = wavefront contribution from test arm without test surface;

$W_S^\alpha$  = wavefront contribution from test surface alone;

$\alpha$  = orientation of wavefront ( $0$  or  $\pi$ ).

In the total absence of errors in the interferometer,  $W_R^\alpha$  and  $W_T^\alpha$  would both be identically zero. In their presence, however,  $W_S^0$  is the desired result and, from the above wavefronts, is determined by computing the following:

$$W_4 = \frac{1}{2}(W_1 + \bar{W}_2) = \frac{1}{2}(W_R^0 + W_R^\pi + W_T^0 + W_T^\pi) + W_S^0,$$

$$W_5 = \frac{1}{2}(W_3 + \bar{W}_3) = \frac{1}{2}(W_R^0 + W_R^\pi + W_T^0 + W_T^\pi).$$

Therefore,

$$W_S^0 = W_4 - W_5.$$

Here, the bar notation denotes transformation of the array of phases equivalent to a rotation of  $\pi$  radians of the wavefronts. Note also that  $W_1$ ,  $W_2$ , and  $W_3$  are wavefronts whose focus and tilt components have been removed. Calculation is performed automatically by the program CAL, and the whole process including setup takes about 5 min.

This now leaves us with two alternatives in the use of the interferometer for testing surfaces or lenses. Either we can use this method to test and correct a master surface to be used as a reference surface or use the above method alone without resorting to comparison with a reference surface. The former approach is initially difficult since the comparison or reference surface must be made to the accuracy desired in the measurement, but only once. Succeeding in this, all subsequent measurements require only the acquisition of two wavefronts and a subtraction—one with the test surface and one with the reference surface. Clearly, if many surfaces were to be measured at the same numerical aperture, the reference surface wavefront would have to be acquired only once and stored in the computer for future comparison with each of the test surfaces. The reference surface wavefront then represents the errors in the interferometer. The technique above represents an alternate means of determining the interferometer errors without the need of a perfect reference surface, but always requires the acquisition of three wavefronts. The needed wavefronts and the result are shown in Fig. 7. An element holder that allows the surface to be accurately rotated by  $180^\circ$  about its center of curvature is also required.

When surfaces are measured, proper orientation must be observed. The plots of concave surfaces appear rotated  $180^\circ$  on the storage display with respect to convex surfaces with the same optical arrangement. Program ALTER may be invoked prior to PLOT so that wavefront display corresponds in a 1:1 fashion with the physical surface.

## VI. Measurement of Spherical Surfaces

An optical system is used in the sample arm to permit the measurement of a wide range of spherical surfaces. An  $f/4$  collimator is used beyond the beam divider to focus the beam at a point as shown in Fig. 2. This point is collimated by a 125-mm diam  $f/4$

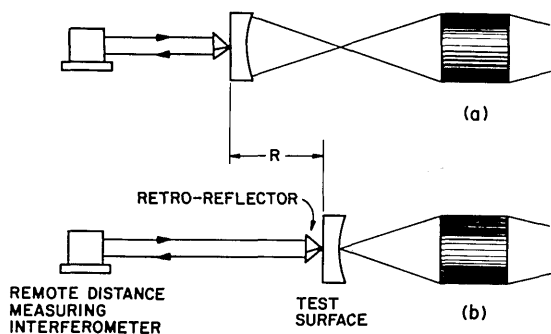


Fig. 8. Setup for measuring radii of curvature with distance measuring interferometer and wavefront correction.

collimator and then imaged by a second identical collimator. Three aplanatic attachments are positioned beyond the second collimator to give an  $f/0.7$  converging cone. Convex surfaces up to 60-mm radius or concave surfaces of any radius can be measured up to this cone angle. When one of the aplanats is removed, convex surfaces up to 120-mm radius and concave surfaces of any radius can be measured with an  $f/1.4$  cone angle. With two aplanats removed 250-mm convex surfaces can be measured with an  $f/2.4$  cone angle. With all three aplanats removed, a convex surface of 450-mm radius can be measured at  $f/4$ . With one collimator removed, flats up to 125-mm diam can be measured, and long radius convex and concave surfaces can be covered by slightly defocusing the first collimator. This allows the majority of surfaces in moderate size optics to be measured.

A reference surface must be measured after each change in this optical system since the interferometer errors will change. The maximum error that is introduced and compensated in this part of the interferometer is  $\lambda/3$ .

## VII. Radius Measurement

A classical technique for radius measurement involves positioning an autocollimator first at the radius of curvature of the surface, then at the apex of the surface, and measuring the distance that the autocollimator (or surface) moves. By measuring wavefronts at these points and tracking the motion of the surface between these points with a distance measuring interferometer, radius measurement to a few parts per million is easily made (cf., Fig. 8). A wavefront is acquired at each position, and the axial focus error at each position is recorded. Knowing the numerical aperture at each of these positions allows the computation of a corresponding sagittal height change. This compensates the error incurred by not precisely positioning the surface at the apex or radius of curvature. The true radius  $R$  is the measurement from the distance measuring interferometer with the correction below.

$$R = R_{\text{COUNTER}} + \delta_2 - \delta_1;$$

$$\delta_i = 2\epsilon_i / (NA_i)^2;$$

$\epsilon_i$  = focus error determined from wavefront measurement;

$NA_i$  = numerical aperture of collimator or surface.

This correction is made with the program DELTA.

The ambient parameters are also considered in this measurement since this effects the laser wavelength. The laser head, remote interferometer and retro-reflector are seen in Fig. 9.

A very significant consequence of both surface and radius measurement with the interferometer is that surfaces of arbitrary radii may be fabricated and tested. The optical shop is thus not tied down to fabrication of only surfaces that are a subset of those test glasses at the facility. Apart from the fact that surfaces tested with test glasses are frequently damaged by contact, the use of a test glass requires that the radius be very close to that of the test glass before the figure can be assessed. Even then, the fringe pattern is very difficult to read to better than  $\lambda/5$  and includes the error in the test glass.

An experiment was conducted in which over forty test glasses were borrowed from reputable optical manufacturers, tested for radius and figure, and returned. The average test glass had errors in figure of  $\lambda/8$  and some as poor as  $\lambda/4$ . Radius errors clustered around 0.5%. These results cast a shadow of doubt on the industry's ability to fabricate or test high quality optics. The details of this experiment will be described in a later paper.

## VIII. Testing a Lens

Lenses for photolithography require diffraction limited performance. Thus, all rays emanating from a point in the object space, passing through the lens, must meet in the image space having transversed equal optical paths within  $\lambda/4$ . This can be measured by placing the lens under test in one of the arms of the interferometer. The interference pattern so obtained is the OPD in the pupil of the lens plus various system errors that can be removed as described below. The simplest method is shown in Fig. 10. First the system errors are computed with the

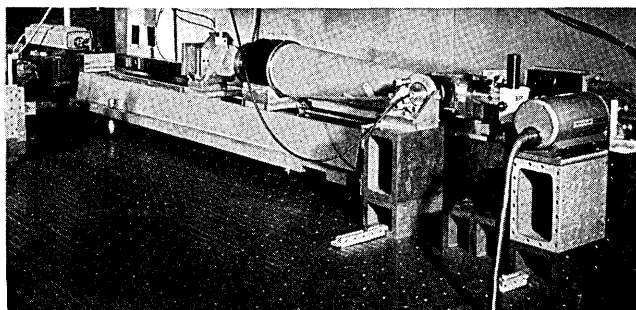


Fig. 9. Wavefront and distance interferometer for radius measurement.

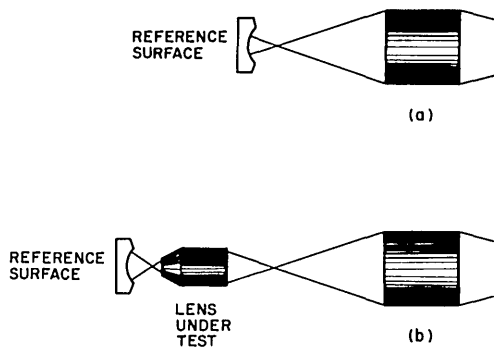


Fig. 10. Lens testing setup (a) for acquiring wavefront of system errors and (b) lens errors plus system errors.

reference surface placed in the test arm as in Fig. 10(a). This wavefront is saved for later subtraction (REF.IN). The lens is then inserted and the reference surface placed on the image side as in Fig. 10(b). The OPD of the lens in single pass is then wavefront (a) minus the wavefront (b). This measurement assumes that the reference surface contributes no error of its own. If the reference surface is not of sufficient quality, the above measurement can be combined with the calibration procedure mentioned previously to establish a correction for the reference surface at each position. The special case of a 1:1 imaging system may be treated with an imperfect reference surface without correction provided the reference surface is rotated 180° between the two positions.

The wavefront in the pupil of the lens is perhaps the most useful indication of lens quality, but other measurements are easily obtainable; these are the point spread function (PSF) and optical transfer function (OTF). The PSF,  $I(x',y')$ , is obtained by taking the Fourier transform of the pupil function  $w(x,y)$ :

$$I(x',y') = A(x',y')A^*(x',y'),$$

$$A(x',y') = \mathbf{F}[w(x,y)] = \int_{\phi} w(x,y) \exp[-2\pi i(x'x + y'y)] dx dy.$$

The inverse transform of the PSF yields the complex OTF.

$$O(f_x, f_y) = \mathbf{F}^{-1}[I(x',y')].$$

The magnitude of the OTF is the more commonly presented result called the modulation transfer function (MTF). This yields the contrast in the image of an object of spatial frequency  $f_x$  or  $f_y$ . Figure 11(a) shows the wavefront in the pupil of a 0.1X lens; Fig. 11(b) shows the derived point spread function in the image; and Fig. 11(c) shows the MTF in the image. Spatial frequency is plotted radially with  $f_x$  the horizontal spatial frequency and  $f_y$  the vertical spatial frequency. Zero frequency is in the center. The spatial frequency for other orientations is also present. Slit scanning techniques employed for MTF

measurement give spatial frequencies in single orientations, whereas processing of wavefront data yields the spatial frequency in all orientations. The phase of the optical transfer function is shown in Fig. 11(d) and indicates the phase shift of higher spatial frequencies from zero frequency. The boundary indicated represents an arbitrary frequency cutoff and is not to be misinterpreted as an aperture.

The Fourier transformations are performed in the minicomputer using the fast Fourier transform (FFT) algorithm. The PSF  $I(x',y')$  is a  $32 \times 32$  real array. This array is imbedded into a  $64 \times 64$  array of zero values and transformed to yield the complex OTF from which the magnitude (MTF) and phase are computed. This imbedding is necessary to prevent aliasing—a consequence of violation of the sampling theorem.

The time required from interferogram to plotted PSF and OTF is less than 1 min for each. More quantitative MTF information is obtained by plotting horizontal and vertical cuts through the MTF surface. These are obtained by executing another program that picks out and interpolates data from the previously computed MTF array. This is shown in Fig. 11(e). The horizontal scale of cycles per millimeter is meaningful when the numerical aperture and wavelength of operation are typed in.

The performance of a truly diffraction limited lens of the same aperture may be easily evaluated by zeroing the wavefront while maintaining the same pupil boundary. This pupil function is then normally processed to yield PSF and OTF information. Thus the effect of wavefront aberration in the presence of vignetting is readily discernible.

The lens bench is shown in Fig. 12. It has been constructed from three movable parts corresponding to the object plane, the lens mount, and the image

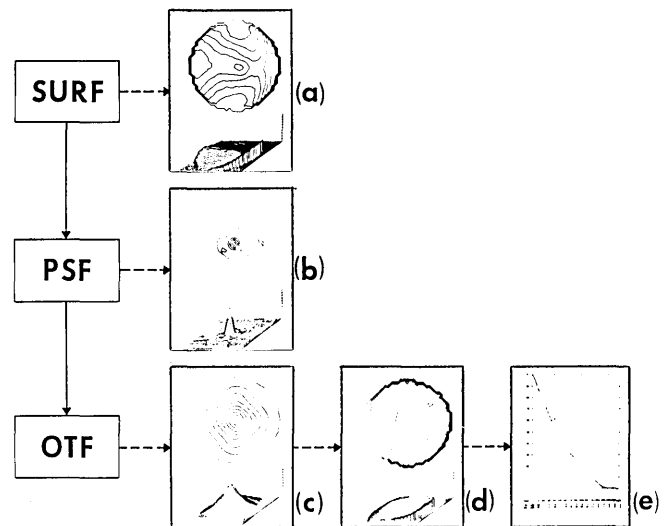


Fig. 11. Performance of a 10X reduction lens measured at 6328 Å and 0.7 of full field position. (a) Wavefront in entrance pupil of lens. (b) Computed point spread function. (c) Modulus and (d) phase of the optical transfer function. The MTF in the two principal planes is plotted in (e).

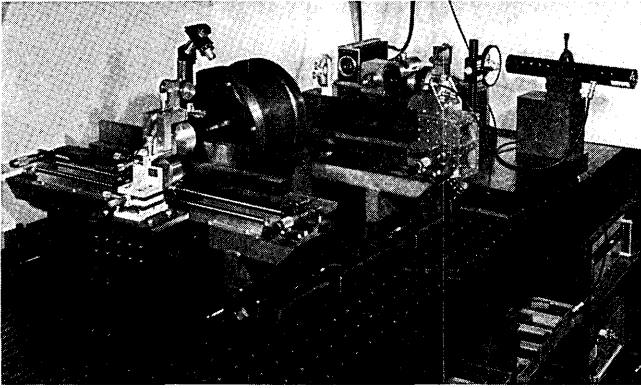


Fig. 12. Lens measurement support. The lens is mounted in the large cylindrical barrel. Object and image planes lie along the knife edges. The interferometer is seen in the background.

plane, respectively. Each is supported on air pads so that small movements can be made easily. Precision scales at the object and image planes allow prelocation of specified field positions. The waist of the beam in the object and image planes is located with respect to the scales by dithering a small tilted screen through focus and observing with a microscope and filar eyepiece. The lens may be rotated and runout with respect to the mechanical mounting noted.

The interferometer is used principally at  $6328 \text{ \AA}$  for both surface and lens testing. Photolithographic lenses are usually tested at the  $4416\text{-\AA}$  HeCd laser line. Lens measurements at wavelengths at which coherent sources may not be available are inferred indirectly by wavefront measurement at  $6328 \text{ \AA}$  and extrapolation using dispersion data of the glasses in the lens. A program has been written that, given the lens design, evaluates the wavefront in the pupil at  $6328 \text{ \AA}$  and punches out a paper tape. The tape is read into the computer and stored. The lens wavefront at  $6328 \text{ \AA}$  is then acquired and its deviation from theory calculated by using the subtraction routine and displaying the result on the storage oscilloscope.

## IX. Conclusions

A real time digital interference pattern measurement scheme has been applied to a Twyman-Green

interferometer. This permits  $\lambda/100$  accuracy with rapid 1:1 display in graphic form of the figure of a surface of OPD of a lens independent of errors in the interferometer optics. Particular attention has been directed to presenting the output in a form most convenient for the technician in the optical shop. Experience with our own shop people has indicated that this is an extremely valuable and necessary tool for the fabrication of precision optics. No question is left in the mind of the technician as to what are the effects of very small changes in polishing strokes or how fast and where material is being removed. Radius measurement to a few ppm may be obtained without contact, freeing the designer to select surface curvatures outside those of available test glasses.

Interferometer control by a dedicated minicomputer permits a basically complex system to be user oriented and very flexible. This software flexibility resulted in programs for data display and manipulation that would not be viable on anything but a real-time system such as this.

Lenses may be tested at various field positions with output in the form of an OPD plot in the pupil, PSF, or modulus and phase of the OTF. Deviations from diffraction limited performance with the same pupil boundary may also be displayed.

The high sensitivity and real time data display have proven to be nearly an indispensable tool in fabrication and testing of truly diffraction limited optics. Furthermore, this has afforded the optician, probably for the first time, direct feedback as to what he is really doing.

The authors gratefully acknowledge helpful discussions with A. Zacharias of Bell Laboratories and the work of Robert Moore of Tropel Inc. for assistance in the software systems programming.

## References

1. J. H. Bruning, J. E. Gallagher, D. R. Herriott, C. L. Nenninger, D. P. Rosenfeld, and A. D. White, "Real Time Wavefront Measurement System for Rapid Display of Surface Quality and Lens Performance," Paper WE16, OSA Meeting (October 1972), San Francisco, Calif.
2. J. H. Bruning and D. R. Herriott, *Appl. Opt.* **9**, 2180 (1970).
3. A. E. Jensen, "Absolute Calibration Method for Laser Twyman-Green Wavefront Testing Interferometers," Paper ThG19, Fall OSA Meeting (October 1973), Rochester, N.Y.